

A theoretical study of the hydrogen-storage potential of $(\text{H}_2)_4\text{CH}_4$ in metal organic framework materials and carbon nanotubes

Q. Li and T. Thonhauser

Department of Physics, Wake Forest University, North Carolina, 27109, USA.

E-mail: thonhauser@wfu.edu

Abstract. The hydrogen-methane compound $(\text{H}_2)_4\text{CH}_4$ —or for short H_4M —is one of the most promising hydrogen-storage materials. This van der Waals compound is extremely rich in molecular hydrogen: 33.3 mass%, not including the hydrogen bound in CH_4 ; including it, we reach even 50.2 mass%. Unfortunately, H_4M is not stable under ambient pressure and temperature, requiring either low temperature or high pressure. In this paper, we investigate the properties and structure of the molecular and crystalline forms of H_4M , using *ab initio* methods based on van der Waals DFT (vdW-DF). We further investigate the possibility of creating the pressures required to stabilize H_4M through external agents such as metal organic framework (MOF) materials and carbon nanotubes, with very encouraging results. In particular, we find that certain MOFs can create considerable pressure for H_4M in their cavities, but not enough to stabilize it at room temperature, and moderate cooling is still necessary. On the other hand, we find that all investigated carbon nanotubes can create the high pressures required for H_4M to be stable at room temperature, with direct implications for new and exciting hydrogen-storage applications.

PACS numbers: 71.15.Mb, 84.60.Ve, 88.30.R-, 61.48.De

Submitted to: *J. Phys.: Condens. Matter*

1. Introduction

The use of hydrogen as an environmentally clean and efficient fuel for mobile applications is a very active research area. But, before a future hydrogen economy can become reality, several crucial challenges need to be addressed, mostly concerning the storage of hydrogen itself [1]. The most important challenges for practical hydrogen-storage system are: (i) high gravimetric and volumetric storage density (fuel tanks should be light and small); (ii) good thermodynamics (the hydrogen adsorption/desorption should occur at a reasonable pressure and temperature); and (iii) fast reaction kinetics (tank emptying and refilling should be fast). According to the Department of Energy, addressing these key elements through fundamental research is imperative to achieving a practical hydrogen economy [2]. In this paper we present results that address the gravimetric and volumetric storage density.

A wide variety of materials have been considered as possible hydrogen-storage materials [3–6] (see Ref. [7] for a graphical representation of how many articles have

been written on the subject). However, amongst all these materials, $(\text{H}_2)_4\text{CH}_4$ —or for short H4M—shows exceptional promise [8]; the H4M system is extremely rich in molecular hydrogen, containing 33.3 mass% molecular hydrogen, not counting the atomic hydrogen in CH_4 ; including it, we reach even 50.2 mass%. Simply said, H4M holds more hydrogen per mass and volume than any known material except pure hydrogen itself! Unfortunately, H4M is not stable under ambient pressure and temperature. The stability field is reported from approximately 5.8 GPa at room temperature to 10 K for ambient pressure [9, 10], and it has been shown that moderate cooling can reduce the required pressure significantly [11]. This fact led us to design a novel host+H4M structure in which the host material provides the necessary pressure for H4M to be stable, without the need for excessive cooling. The use of a host material will lower the exceptional volumetric and gravimetric hydrogen storage density of H4M—it is the main goal of this paper to quantify the tradeoff between lower storage density and stability at closer-to-ambient temperature and explore if it is worth pursuing.

Since H4M is stable at room temperature under a pressure of 5.8 GPa, we are most interested in this region of the phase diagram and throughout the manuscript we report results at that pressure. We first consider H4M in nanoporous metal organic framework (MOF) materials [12–15], which provide significant pressure inside their cavities to stabilize H4M. We study MOFs that are isorecticular to (i.e. have the same network topology as) MOF-5, with varying linker length. We find that these MOFs all provide enough pressure to significantly decrease the burden of cooling, but none of them stabilize H4M at room temperature. As a second host material, we consider single-wall carbon nanotubes (CNT) [16], which are well known for being able to provide high pressure inside their cavities. Specifically, we study zigzag nanotubes with chirality from (10,0) to (26,0) and corresponding radii from 4 Å to 10 Å—while larger nanotubes with a radius up to several nanometers can be produced in experiments [17], such systems together with H4M filling inside are, at the moment, not accessible through *ab initio* simulations. Our calculations show that crystalline H4M may be stabilized at room temperature inside nanotubes, opening the door for high-efficiency hydrogen-storage applications.

This paper is organized as follows: After presenting computational details in section 2, we show results for the structure of H4M in its molecular and crystalline form in section 3. Results for H4M inside the cavities of MOFs and nanotubes are presented in section 4 and 5, respectively. We conclude and suggest future research in section 6.

2. Computational Details

H4M is classified as a van der Waals compound [9]. The study of nanotube interactions [18] and binding of small molecules in MOFs [19] is also strongly determined by van der Waals interactions. As such, an accurate description of van der Waals interactions in these systems is crucial. Thus, we use the recently developed van der Waals density functional (vdW-DF), a truly nonlocal exchange and correlation functional, that incorporates van der Waals forces self-consistently and seamlessly into DFT [20–22]. The vdW-DF approach has shown good transferability for a range of van der Waals systems reaching from simple dimers [23] and physisorbed molecules [24] to DNA [25] and drug design [26]. In particular, it has been applied successfully to answer questions regarding hydrogen storage [27], MOFs [19], and nanotubes [18].

For our calculations we use density functional theory, as implemented in the PWSCF code, which is part of the QUANTUM-ESPRESSO package [28]. We utilize ultrasoft pseudopotentials with a wave-function cutoff of 475 eV (5700 eV charge-density cutoff) for carbon nanotube related systems and 475 eV (3800 eV charge-density cutoff) for all other cases. A self-consistency convergence criterion of at least 1.4×10^{-7} eV is used. All structures are relaxed until all force components are less than 2.5 meV/Å. Due to the limitation of calculation size, and the fact that larger MOFs provide less pressure anyway, only the smallest MOF structures are investigated, using a $2 \times 2 \times 2$ Monkhorst-Pack \mathbf{k} -mesh [29]. For simulations of crystalline H4M itself, we use a $4 \times 4 \times 4$ \mathbf{k} -mesh. All carbon nanotube related systems are simulated as infinitely long hexagonal nanotube arrays with varying radius/distance, comprised of a short unit cell length in z -direction, using a $1 \times 1 \times 16$ \mathbf{k} -mesh. Single molecule calculations on H4M molecules are performed in a $16 \times 16 \times 16$ Å³ cubic unit cell.

3. Structure of H4M

Although H4M under pressure has been investigated by X-ray diffraction [10], the actual microscopic structure of crystalline H4M remains unknown [9]. The X-ray diffraction experiments suggest a body-centered tetragonal structure [10] and Raman experiments provide further constraints [9]. Here, starting from these experimental guidelines, we report results for *ab initio* calculations of the molecular and crystalline H4M structure. We use a bottom-up approach, where we first find the optimal structure for H4M molecules, which we then assemble to form solids with various symmetries.

3.1. Structure of molecular H4M

We start by investigating the structure of a single H4M molecule. After relaxing the molecule, starting from a variety of initial positions, we always find the same optimal structure: the molecule forms two tetrahedra, sharing the same center with opposite directions. The common center is the carbon atom of the methane molecule, which forms the small tetrahedron. The four hydrogen molecules form a larger tetrahedron, each of them located on one of the vertexes, and oriented so that they point to the central carbon atom of the methane. We find the C–H bond of the methane molecule to be 1.091 Å, the H–H bond of the hydrogen molecules to be 0.742 Å, and the distance from the central carbon atom to the closer hydrogen atom of the hydrogen molecules to be 3.295 Å. The optimized structure of the H4M molecule is depicted in figure 1.

In table 1, we list the binding energy as a function of the number of H₂ molecules bound to the central CH₄ molecule. Here, the binding energy is defined as $E_{\text{bind}} = E[(\text{H}_2)_n\text{CH}_4] - E[\text{CH}_4] - n E[\text{H}_2]$ for the case of n H₂ molecules bound to the CH₄ molecule. We can see that an increase in the number of H₂ molecules leads to an increase in binding energy per H₂ molecule, due to the additional interaction of H₂ molecules. We also report the incremental absorption energy, i.e. the work to absorb each new H₂ molecule. The increasing magnitude in both columns validates the stability of the H4M molecule.

At this point, it is instructive to pause for a moment and analyze the performance of vdW-DF in H4M, the structure and binding of which is very much determined by van der Waals forces. Since this molecule is small enough, we can compare here with

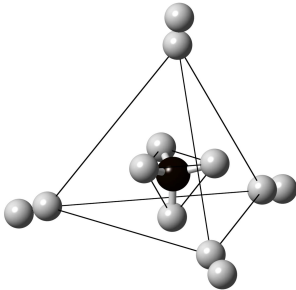


Figure 1. Optimized structure of a single H4M molecule $(\text{H}_2)_4\text{CH}_4$. The methane molecule forms a small tetrahedra, which sits inside a large tetrahedra formed by the hydrogen molecules. The axes of all hydrogen molecules point toward the centers of faces of the methane tetrahedra.

Table 1. Binding energies E_{bind} [meV] of H_2 in $(\text{H}_2)_n\text{CH}_4$ as a function of the number of H_2 molecules attached. We also report the incremental absorption energy $E_{\text{abs}}^{\text{inc}}$ [meV], i.e. the work to absorb each new H_2 molecule.

n	E_{bind}	$E_{\text{bind}}/\text{H}_2$	$E_{\text{abs}}^{\text{inc}}$
1	-19.50	-19.50	-19.50
2	-39.58	-19.79	-20.08
3	-60.33	-20.11	-20.75
4	-81.36	-20.34	-21.03

the highest level of quantum chemistry. To this end, we have calculated the binding energy of four H_2 molecules to methane—i.e. the last row of table 1—using various approaches and exchange-correlation functionals. As reference, we use MP2 and CCSD(T) calculations, using the aug-cc-pVDZ basis set with counterpoise corrections. For the binding energy we find -85.93 meV with MP2 and -87.75 meV with CCSD(T). These reference numbers are now to be compared with DFT calculations. Using standard LDA [30], we find a very strong erroneous overbinding of -194.37 meV, not untypical when applying LDA to small molecules with van der Waals binding [31]. On the other hand, a standard PBE [32] calculation gives a large erroneous underbinding of only -36.65 meV. From these results it is clear that a simple H4M molecule is a very delicate system that is very much influenced by van der Waals interactions and thus an ideal application for vdW-DF. The corresponding binding energy with vdW-DF is -81.36 meV, in almost perfect agreement with high-level quantum chemistry. These results show that standard functionals such as LDA and PBE are not suited to describe the binding of H4M itself and much less so to study the H4M crystal structure or its properties inside MOFs and nanotubes; thus, in the following we will only report results for vdW-DF.

Also worth mentioning at this point is that vdW-DF is responsible for a small but significant charge transfer; in fact, it seems that vdW-DF is self-consistently rearranging the charge density just right, resulting in the excellent binding energy. Such charge transfers caused by vdW-DF are typically very small, i.e. on the order of 10^{-4} electrons/ \AA^3 , where electronic charge gets accumulated between the constituents. A nice presentation of this charge transfer due to van der Waals binding is given in figure 8 of Ref. [21].

3.2. Structure of crystalline H4M

To find the true crystalline structure for H4M is a complicated task. In principle, one should use an approach such as the *ab initio* random structure search (AIRSS) algorithm [33]—which generates random structures biased on chemistry, experimental, and symmetry grounds—to sample the corresponding large phase space. Here, however, we make use of experimentally suggested symmetries [9,10] and an already existing semiclassical sampling of a large number of possible configurations [34].

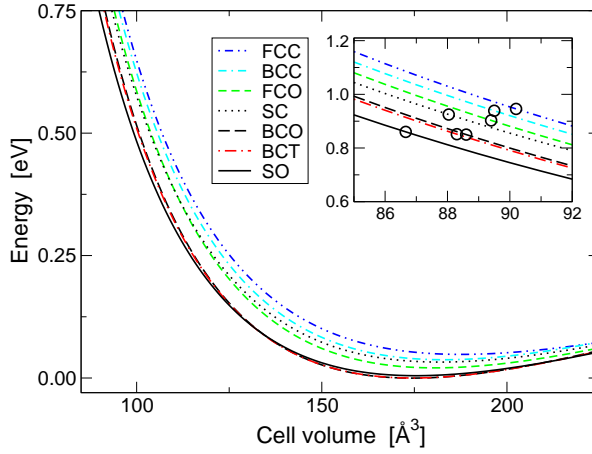
After Somayazulu et al. suggested a body-centered tetragonal (BCT) structure (with some uncertainty) based on X-ray diffraction patterns [10], research on the precise structure of crystalline H4M seems to have subsided. Fifteen years later, Mao et al. found a simple orthorhombic unit cell for crystalline H4M from a combined semiclassical/DFT approach by randomly arranging atoms, which resulted in a good agreement between calculated and experimental XRD spectra [34]. They found an optimized unit cell of 332 Å³ with four H4M molecules, resulting in a molecular hydrogen volumetric density of 0.16 kg H₂/L, in disagreement with their previously published number, which is almost twice as large [8]—which we thus believe to be an error.

Using the above information as starting point, we generate seven closely related possible unit cells with an H4M molecule as a building block (using the molecular structure described above), i.e. simple/body-centered/face-centered cubic (SC/BCC/FCC), simple/body-centered/face-centered orthorhombic (SO/BCO/FCO), and body-centered tetragonal (BCT). For all seven structures, we internally (atom positions) and externally (unit cell parameters) optimize the unit cells and determine the optimal ratios between the lengths of their edges (b/a and c/a) without pressure; the corresponding results are listed in table 2. Then, we add hydrostatic pressure by changing the cell parameter a , while keeping b/a and c/a constant, and relaxing the atom positions again for each volume. Applying the exact conditions of hydrostatic pressure requires knowledge of all corresponding elastic constants, but test calculations show that H4M is close to isotropic, such that the uniform scaling of all lattice constants is a good approximation[‡]. The resulting energy versus volume curves are fitted using a Murnaghan equation of state, enabling us to analyze the structures and their pressure dependence in detail; results are shown in figure 2. As can be seen, the BCO and BCT curves are very close to each other due to the similarity of their structures, and they have the lowest energies at zero pressure. However, as the pressure increases, they cross with the SO curve, indicating a pseudo-phase transformation at around 1.8 GPa. At 5.8 GPa—the pressure at which H4M is experimentally stable at room temperature—SO has the smallest volume and slightly higher energy than BCO/BCT. Since at zero temperature the condition for the stable structure at constant pressure is that enthalpy ($H = E + PV$) be minimum [35], we conclude that the SO structure is favored at 5.8 GPa, in agreement with Mao et al. [34]. The corresponding results for zero pressure and a pressure of 5.8 GPa are listed in table 3. It is striking to see how “soft” this material is, as evident by the tremendous volume change upon applying 5.8 GPa of pressure, as is expected for a van der Waals crystal.

[‡] E.g. the SO unit cell is almost tetragonal—see table 2—and our calculations show that the corresponding elastic constants c_{22} and c_{33} differ only by a few percent, while c_{33} differs by about 10%. The numbers are similar for other symmetries.

Table 2. Lattice constant a [\AA] and corresponding ratios b/a and c/a for crystalline H4M in various symmetries.

Symmetry	a @ 5.8 GPa	a @ 0 GPa	b/a	c/a
FCC	7.119	9.089	1	1
BCC	5.636	7.166	1	1
FCO	7.791	9.865	0.897	0.843
SC	4.449	5.684	1	1
BCO	6.162	7.741	0.976	0.776
BCT	6.056	7.628	1	0.795
SO	5.174	6.567	0.798	0.784

**Figure 2.** Energy versus volume curve for seven possible symmetries of the H4M crystal. The circles in the small inset indicate the 5.8 GPa point of each structure. Energies are plotted relative to the SO energy at zero pressure.**Table 3.** Volume V [\AA^3], volumetric hydrogen density ρ_{vol} [$\text{kg H}_2/\text{L}$], energy E [meV], and enthalpy H [meV] of crystalline H4M for various symmetries. Energies are reported relative to the values for the SO structure.

Symmetry	@ 5.8 GPa				@ 0 GPa		
	V	ρ_{vol}	E	H	V	ρ_{vol}	E
FCC	90.19	0.1473	88.2	215.9	187.68	0.0708	42.8
BCC	89.49	0.1484	80.5	182.9	184.01	0.0722	32.0
FCO	89.40	0.1486	44.4	143.6	181.47	0.0732	15.4
SC	88.04	0.1509	65.1	114.9	183.62	0.0723	27.4
BCO	88.59	0.1499	-8.1	61.7	175.63	0.0756	-5.3
BCT	88.31	0.1504	-7.3	52.1	176.45	0.0753	-5.3
SO	86.67	0.1533	0.0	0.0	177.16	0.0750	0

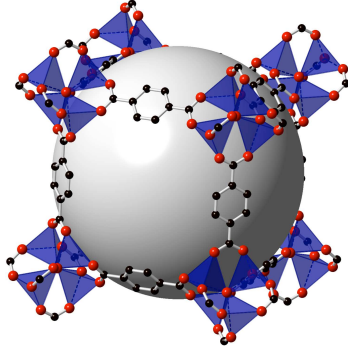


Figure 3. Structure of MOF-5. The unit cell consists of 424 atoms (for clarity hydrogen atoms are not displayed). The Zn–O–C clusters at the corners are connected through one benzene linker. The sphere in the middle serves as a measure for the size of the cavity—we refer to the radius of this sphere as the *fixed radius*. The *free radius* is defined as the radius of the largest sphere that fits through the aperture.

4. H4M in MOFs

With the H4M crystal structure, we are now ready to position H4M into external host materials, in the hope to stabilize it at reasonable temperatures. We begin by investigating the possible pressure range that several common MOF materials exhibit. For our study, we limit ourselves to three MOFs of different sizes. The smallest MOF we include is MOF-5, consisting of Zn–O–C clusters at the corners, connected through one benzene linker in a cubic symmetry, depicted in figure 3. From this starting structure, larger MOFs can be built by simply making the chain of benzene linkers longer, while keeping the network topology the same. Such MOFs are referred to as *isoreticular*, and we have selected irMOF-10 (the linker chain contains two benzene rings) and irMOF-16 (the linker chain contains three benzene rings). For a nice graphical representation and further details of the three MOFs under investigation, please see Ref. [15]. As the starting point for the three MOF structures, we use experimental atom positions from the supplementary materials of Ref. [15].

MOFs can have very large unit cells with hundreds of atoms, which—together with hundreds of atoms from the H4M filling—can quickly render *ab initio* calculations impractical. In order to still be able to make quantitative statements, we begin by investigating empty MOFs and the pressure they can create in their cavities. With the knowledge gained about MOF strength, we estimate their performance when filled with H4M. We verify the results with one full *ab initio* calculation on a small, but complete system of MOF+H4M.

First, we investigate the strength of the bond between the Zn–O–C cluster corners and the connected benzene linker. Knowing the strength of this bond allows us to estimate the pressure the MOF can withstand in its cavity. To this end, we perform total energy calculations in which we pull the benzene ring away from the cluster. We keep the structure in x and y directions constant, and move the benzene ring along the z -axis. To accommodate this, we construct a new tetragonal unit cell with the same cell parameter in x and y directions (12.916 Å) as the relaxed cubic MOF-5 structure, but with an elongated z -edge with a c/a value of 2.2. This allows us to move the benzene ring several Å, while always keeping a minimum distance of

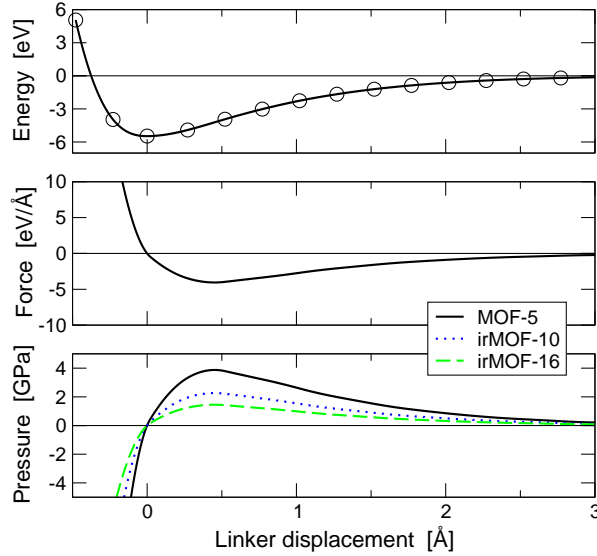


Figure 4. Energy and calculated force/pressure versus benzene ring displacement in z -direction of simulated MOF-5. The energy is plotted relative to the energy of the completely separated Zn–O–C cluster and benzene ring. In the upper panel, open circles indicate the *ab initio* results; the solid lines are spline fittings.

at least 8 Å to the Zn–O–C cluster in the next unit cell. The side of the benzene that would usually connect to the next corner was hydrogen terminated. Throughout the calculations, the relative positions of the atoms in the Zn–O–C cluster and the benzene rings are fixed, the only element that changes is the relative distance between the Zn–O–C cluster and the benzene ring in the z -direction. Results of the total energy versus benzene ring displacement are plotted in the upper panel of figure 4. The force is then calculated by the energy derivative and is plotted in the middle panel of figure 4. From this, we can estimate the possible pressure that MOF-5 can create, as the pressure is the ratio between the force and the area of the square in the cubic unit cell. Note that the connection of the benzene ring to the Zn–O–C clusters at the corners is the same for MOF-5, irMOF-10, and irMOF-16. As such, the energy vs. benzene ring displacement plot allows us to estimate the pressure for all three MOFs. Simple test calculations show that the bond between two benzene rings in longer linkers is slightly stronger than the bond between the Zn–O–C cluster and the first benzene ring. In other words, the bond between the Zn–O–C cluster and the first benzene ring breaks before the bond between two benzene linkers. Thus, the corresponding pressure in irMOF-10 and irMOF-16 can easily be estimated by dividing by their corresponding (larger) areas. The pressures, as a function of benzene ring displacement, estimated in this way are depicted in the lower panel of figure 4. The zero point on the horizontal displacement axis indicates the position at which the benzene linker sits in the optimized zero-pressure unit cell. The maximum pressure in the case of MOF-5 is 3.9 GPa, close to the required H4M storage pressure at room temperature. The larger host materials irMOF-10 and irMOF-16 can still produce a maximum pressure of 2.3 GPa and 1.5 GPa, respectively, before they break.

We next investigate the possible storage of H4M in these MOF systems. The free and fixed diameter (see figure 3 for a definition of these terms) of the pores in MOF-5

Table 4. Performance of different MOFs as hosts for H4M. Given are: MOF type, free and fixed pore diameter [Å], maximum commensurate size of the H4M supercell for filling, hydrogen mass density ρ_{mass} [mass%] with and without the hydrogen in CH₄, maximum pressure P achievable [GPa], and temperature T [K] to which systems needs to be cooled to stabilize H4M.

System	Free	Fixed	Filling	$\rho_{\text{mass}}^{\text{w}}$	$\rho_{\text{mass}}^{\text{w/o}}$	Max. P	T
MOF-5	11.2	18.6	$2 \times 2 \times 2$	10.0	6.7	3.9	224
irMOF-10	15.4	24.5	$3 \times 3 \times 3$	19.5	13.0	2.3	172
irMOF-16	19.1	28.8	$3 \times 3 \times 3$	15.3	10.2	1.5	126
Pure H4M	—	—	—	50.2	33.3	—	10

have been reported as 11.2 Å and 18.6 Å, respectively [15]. Since the diagonal length of our calculated SO H4M structure at 5.8 GPa is 7.7 Å, we insert a $2 \times 2 \times 2$ compressed H4M supercell into the pores of MOF-5. The MOF-5 structure itself has 424 atoms; fully filled with the H4M supercell, this corresponds to more than 1000 atoms. Since this is computationally too demanding, we only fill one pore (out of eight) per unit cell, resulting in a 528 atom unit cell. We then perform *ab initio* calculations on this system and find that the unit cell experiences a pressure of 3.9 GPa (the fact that this number is the same as the corresponding maximum pressure in table 4 is accidental.) This pressure is lower than the 5.8 GPa compacted H4M supercell that inserted, simply because the cavity is slightly larger than the H4M supercell. When we further let all atoms relax again in this structure, we find that the unit cell stabilizes at approximately 1 GPa. Note that, upon relaxation, we find only minimal changes in the atoms positions of both the MOF and the inserted H4M.

Based on the estimations from above, in table 4, we list the theoretical performance of H4M storage in MOF-5, irMOF-10, and irMOF-16. Since the pore size should be approximately commensurate with the unit cell size of crystalline H4M, we can estimate a possibly largest H4M supercell that would fit in each pore, according to the pore diameters [15]. From that, we calculate the hydrogen mass density—including and not including the hydrogen in CH₄. In addition, with the knowledge of the experimentally determined stability field [9] and the possible maximum pressure from above, we estimate to which temperature the systems need to be cooled for the H4M to be stable. Overall, there is a trade-off between the cooling required and mass density—the higher the hydrogen mass density is, the more cooling is required. Even though none of those three MOFs stabilize H4M at room temperature, these results are promising: experimentally, pure hydrogen gas absorption using MOF-5 can reach a maximum mass density of 4 mass% [13], while our calculated hydrogen mass density—using H4M as a guest molecule—is significantly higher. This result is related to the fact that most of the pure hydrogen molecules physisorb on the inside walls of the pores, while using H4M makes more efficient use of the entire pore volume.

5. H4M in nanotubes

Nanotubes have been studied extensively and it is well known that they have extraordinary electronic and physical properties [16]. In particular, nanotubes have exceptional high stiffness and strength and hence the ability to withstand large elastic strain [36, 37]. In the following, we investigate if carbon nanotubes can

provide the necessary pressure to stabilize H4M. We consider zigzag single-wall carbon nanotubes—since they are semiconducting and thus easier to model—with chirality (n, m) ranging from $(10, 0)$ to $(26, 0)$, corresponding to radii from 4 Å to 10 Å. While larger nanotubes with a radius of up to several nanometers can be produced in experiments [17], the filling of such systems with H4M is currently not accessible through *ab initio* simulations, due to the large number of atoms. Similar to the case of H4M in MOFs, we first model empty nanotubes to find their elastic properties and then investigate their loading with H4M through suitable approximations. Again, we verify our results by one *ab initio* calculation on a small, but complete system of CNT+H4M.

5.1. Radial Young's modulus and strain of carbon nanotubes

The property of most interest to us is the Young's modulus, as it is closely related to the pressure resulting from a small perturbation to the tube's radius. Since the axial Young's modulus has been determined to be 1 TPa [37, 38], we focus on the radial Young's modulus here. We start from the properties of isolated carbon nanotubes, modeling them with a minimum wall-to-wall separation of at least 8 Å. The radial Young's modulus E_r in a hydrostatic pressure model is given by

$$\Delta U_e = \frac{E_r A_0 \Delta r^2}{2r_0}, \quad (1)$$

where ΔU_e is the relative strain energy, A_0 and r_0 are the original cross-section and radius, and Δr is the amount by which the radius changes. For each nanotube, we first relax the structure and then perform five self-consistent calculations varying the tube radius by 0%, $\pm 0.5\%$, and $\pm 1\%$. As expected, ΔU_e and Δr satisfy a quadratic relation in a small vicinity of r_0 , allowing us to calculate E_r for each nanotube. Our results are depicted in figure 5, together with recently reported results from analytical calculations [39], where the following fit for E_r of zigzag carbon nanotubes has been found:

$$E_r = \frac{2nk_s \sin^2(\pi/n)}{3\pi b}. \quad (2)$$

Here, n , b , and k_s refer to the chirality $(n, 0)$, the C–C bond length (in our case 1.42 Å), and the stretching force constant of the covalent bond. The comparison of our results to the results of Li et al. [39] is already very good, but can be improved if we adjust k_s from its originally published value of 652 N/m to 610 N/m.

Knowledge of the radial Young's modulus allows us to estimate which pressure the nanotubes can withstand inside its cavity. In particular, we use the Young's modulus found previously, to calculate the strain necessary to create 5.8 GPa of pressure inside the nanotube—this is the pressure required to stabilize H4M at room temperature. The corresponding strains are given in table 5. Next, we perform simple calculations on the carbon framework to measure how much strain it can withstand before it breaks. In our calculations we investigate strains from 10% to 20% and we find that the carbon network breaks approximately at 15% strain, in good agreement with Ref. [40, 41]; although other experiments note that breaking occurs at a lower strain of around 5% [37, 42].

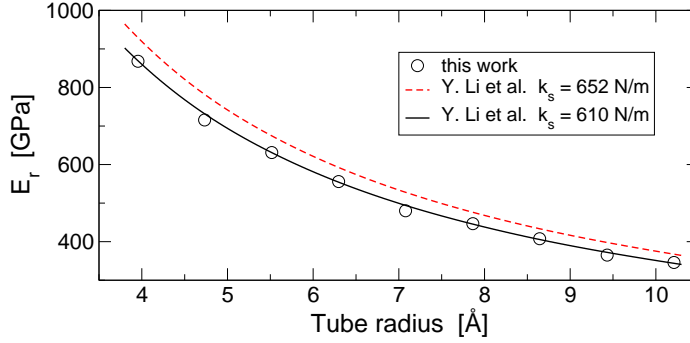


Figure 5. Calculated radial Young's modulus of nanotubes of different sizes.

5.2. Binding between nanotubes, optimized separation for a nanotube bundle

We next investigate the binding of nanotubes to each other. To this end we arrange the nanotubes in a hexagonal unit cell and study the energy as a function of separation in such bundles. We start from isolated nanotubes and bring them together incrementally, performing two types of calculations: (i) the atoms in the tubes are fixed and (ii) the tubes are free to deform. From the resulting energy curves, we find that nanotubes bind approximately at a wall-to-wall separation of 3.5 \AA , nearly independent of size. Furthermore, larger tubes undergo more deformation at close distance and there is a significant energy gain from the deformation if the separation is less than 3 \AA for tubes with chirality larger than $(16,0)$. Since the deformation only plays a significant role in a region closer than the natural binding distance, we will use a 3.5 \AA wall-to-wall distance and start all simulations from undistorted nanotubes in the calculations reported below. From our calculated wall-to-wall separation of nanotubes in bundles, we can then deduce the achievable volumetric hydrogen-storage density; results are given in table 5.

5.3. CNT+H4M system

The length of one of the edges of the SO H4M crystalline unit cell at 5.8 GPa is very close to the unit cell length of carbon nanotubes in axial direction (4.27 \AA). Hence, we compress the H4M unit cell slightly so that the edge is exactly commensurate and scale the other two edges accordingly. We then put $n \times n \times 1$ supercells of H4M inside the carbon nanotubes and relax the whole system. For example, since the diagonal length of the scaled H4M unit cell is 6.6 \AA (slightly bigger than the radius of the $(16,0)$ carbon nanotube), it is natural to build the filled structure from a $(16,0)$ nanotube together with a $2 \times 2 \times 1$ H4M supercell. We slightly adjust the position of several hydrogen molecules at the corners to prevent steric clashes. The resulting relaxed structure is shown in figure 6. Throughout the relaxation, the structure of H4M changes noticeably. The nanotube also deforms and exhibits a strain of 1.4%, which is more than we estimated in table 5 since we compressed the supercell slightly to make it commensurate; but nevertheless, it withstands the pressure created by the H4M inside.

In table 5, we list the theoretically possible hydrogen mass density for the CNT+H4M system for nanotubes up to a radius of 25 \AA ; even better performance

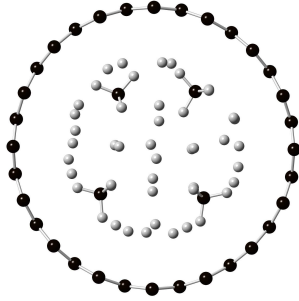


Figure 6. Optimized structure of a $2 \times 2 \times 1$ supercell of H4M inside a (16,0) carbon nanotube.

Table 5. Theoretically predicted performance of the CNT+H4M systems. Given are the chirality of the system, the nanotube radius [\AA], the largest possible H4M supercell commensurate with the diameter, the mass densities ρ_{mass} (with and without including the hydrogen in CH_4) [mass%], the volumetric densities ρ_{vol} [$\text{kg H}_2/\text{L}$], the radial Young’s modulus E_r [GPa], and the strain ε [%] required to produce 5.8 GPa.

System	Radius	Filling	$\rho_{\text{mass}}^{\text{w}}$	$\rho_{\text{mass}}^{\text{w/o}}$	ρ_{vol}	E_r	ε
(10,0)	3.95	$1 \times 1 \times 1$	2.4	1.6	0.028	870	0.7
(16,0)	6.30	$2 \times 2 \times 1$	5.6	3.7	0.055	555	1.0
(24,0)	9.43	$3 \times 3 \times 1$	7.9	5.3	0.065	373	1.6
(32,0)	12.56	$4 \times 4 \times 1$	10.0	6.7	0.070	280	2.1
(40,0)	15.69	$5 \times 5 \times 1 + 8$	14.6	9.7	0.097	224	2.6
(48,0)	18.82	$6 \times 6 \times 1 + 12$	16.7	11.1	0.102	187	3.1
(56,0)	21.96	$7 \times 7 \times 1 + 16$	18.4	12.2	0.103	160	3.6
(64,0)	25.08	$8 \times 8 \times 1 + 24$	20.4	13.6	0.110	140	4.1
H4M	—	—	50.2	33.3	0.160	—	—

might be achievable for larger tubes. Note that for tubes starting at (40,0), the filling with supercells of H4M is not simply a square-type pattern corresponding to $n \times n \times 1$, but we can fit in further unit cells on the side to better approximate the circular shape of the tube. The corresponding filling is then reported as $n \times n \times 1 + m$, where m indicates the number of additional unit cells of H4M that we are able to fit in a given tube. According to our estimation, all indicated tubes provide enough pressure to stabilize H4M at room temperature.

6. Conclusions

In this paper we present results of *ab initio* calculations on the H4M system for the purpose of hydrogen storage. While H4M shows exceptional hydrogen mass storage density—well beyond the required Department of Energy target—it falls short in its thermodynamic properties. It requires either very high pressure to be stable at room temperature, or it needs to be extensively cooled at ambient pressure. Our *ab initio* simulations are a proof of concept that external agents such as MOFs and carbon nanotubes can be used to provide the necessary pressure. We find that certain MOFs provide enough pressure to significantly decrease the burden of cooling, but none

of them stabilize H4M at room temperature. On the other hand, we find the very encouraging result that carbon nanotubes may stabilize H4M at room temperature with outstanding gravimetric and volumetric hydrogen storage densities.

While in this study we have performed basic simulations of possible host materials to stabilize H4M, we have not addressed related practical issues. Questions arise such as: even if these host materials are, in principle, capable of stabilizing H4M at close-to-ambient temperatures, how can we practically place the H4M inside the cavities of these host materials? Also, it is not clear that the radial pressure of the nanotubes alone is practically enough to stabilize H4M, some axial pressure might be necessary. More research is needed to see if H4M can be crystallized inside these structures, or if it can form clusters at a low temperature and then diffuse into these cavities.

Acknowledgments

We would like to dedicate this report to the memory of *Prof. David Langreth*, who passed away in mid-2011—he is the “father” of vdW-DF and his research inspired many. All calculations were performed on the WFU DEAC cluster. This work was supported by the Department of Energy Grant, Office of Basic Energy Sciences, Materials Sciences and Engineering Division, Grant No. DE-FG02-08ER46491.

References

- [1] US Department of Energy, Basic Energy Sciences Advisory Committee 2003: *Basic Research Needs to Assure a Secure Energy Future* (Washington DC). Retrieved from http://science.energy.gov/~media/bes/pdf/reports/files/sef_rpt.pdf
- [2] US Department of Energy, Office of Basic Energy Sciences 2004: *Basic Research Needs for the Hydrogen Economy*, (Washington DC). Retrieved from http://science.energy.gov/~media/bes/pdf/reports/files/nhe_rpt.pdf.
- [3] Züttel A 2004 *Naturwissenschaften* **91** 157
- [4] Crabtree G W, Dresselhaus M S and Buchanan M V 2004 *Phys. Today* **57** 39
- [5] Lim K L, Kazemian H, Yaakob Z and Daud W R W 2010 *Chem. Eng. Technol.* **33** 213
- [6] Sakintuna B, Lamari-Darkrim F and Hirscher M 2007 *Int. J. Hydrogen Energy* **32** 1121
- [7] Makowski P, Thomas A, Kuhn P and Goettmann F 2009 *Energy Environ.* **2** 480
- [8] Mao W L, Koh C A and Sloan E D 2007 *Phys. Today* **60** 42
- [9] Mao W L, Struzhkin V V, Mao H and Hemley R J 2005 *Chem. Phys. Lett.* **402** 66
- [10] Somayazulu M S, Finger L W, Hemley R J and Mao H K 1996 *Science* **271** 1400
- [11] Mao W L and Mao H K 2004 *Proc. Nat. Aca. Sci.* **101** 708
- [12] Yaghi O M, Li G and Li H 1995 *Nature* **378** 703
- [13] Rosi N L, Eckert J, Eddaoudi M, Vodak D T, Kim J, O’keeffe M and Yaghi O M 2003 *Science* **300** 1127
- [14] Zhao X, Xiao B, Fletcher A J, Thomas K M, Bradshaw D and Rosseinsky M J 2004 *Science* **306** 1012
- [15] Eddaoudi M, Kim J, Rosi N, Vodak D T, Wachter J, O’Keeffe M and Yaghi O M 2002 *Science* **295** 469
- [16] Dresselhaus M S, Dresselhaus G and Eklund P C 1996 *Science of Fullerenes and Carbon Nanotubes: Their Properties and Applications*, Academic Press, New York
- [17] Cheung C L, Kurtz A, Park H and Lieber C M 2002 *J. Phys. Chem. B* **106** 2429
- [18] Román-Pérez G and Soler J M 2009 *Phys. Rev. Lett.* **103** 096102
- [19] Yao Y, Nijem N, Li J, Chabal Y J, Langreth D C and Thonhauser T 2012 *Phys. Rev. B* in print
- [20] Dion M, Rydberg H, Schröder E, Langreth D C and Lundqvist B I 2004 *Phys. Rev. Lett.* **92** 246401; 2005 **95** 109902(E)
- [21] Thonhauser T, Cooper V R, Li S, Puzder A, Hyldgaard P and Langreth D C 2007 *Phys. Rev. B* **76** 125112
- [22] Langreth D C *et al.* 2009 *J. Phys. Condens. Matter* **21** 084203
- [23] Thonhauser T, Puzder A and Langreth D C 2006 *J. Chem. Phys.* **124** 164106; Li S, Cooper V R, Thonhauser T, Puzder A and Langreth D C 2008 *J. Phys. Chem. A* **112** 9031; Hooper J,

- Cooper V R, Thonhauser T, Romero N A, Zerilli F and Langreth D C 2008 *ChemPhysChem* **9** 891
- [24] Mura M, Gulans A, Thonhauser T and Kantorovich L 2010 *Phys. Chem. Chem. Phys.* **12** 4759
- [25] Cooper V R, Thonhauser T, Puzder A, Schröder E, Lundqvist B I and Langreth D C 2008 *J. Am. Chem. Soc.* **130** 1304; Cooper V R, Thonhauser T and Langreth D C 2008 *J. Chem. Phys.* **128** 204102
- [26] Li S, Cooper V R, Thonhauser T, Lundqvist B I and Langreth D C 2009 *J. Phys. Chem. B* **113** 11166
- [27] Li Q, Kolb B, Román-Pérez G, Soler J M, Yndurain F, Kong L, Langreth D C and Thonhauser T 2011 *Phys. Rev. B* **84** 153103
- [28] P. Giannozzi *et al.* 2010 *J. Phys. Condens. Matter* **22** 022201
- [29] Pack J D and Monkhorst H J 1976 *Phys. Rev. B* **13** 5188; 1977 **16** 1748
- [30] Perdew J P and Wang Y 1992 *Phys. Rev. B* **45** 13244
- [31] Kolb B and Thonhauser T 2011 *Phys. Rev. B* **84** 045116
- [32] Perdew J P, Burke K and Ernzerhof M 1996 *Phys. Rev. Lett.* **77** 3865
- [33] Pickard C J and Needs R J 2011 *J. Phys.: Condens. Matter* **23** 053201
- [34] Mao W L *et al.* 2009 *Global Climate & Energy Project Symposium 2009*, available at http://gcep.stanford.edu/pdfs/CT1SZRP4nww_77Shjd-A2g/WendyMao_Symposium2009.pdf
- [35] Martin R M 2004 *Electronic Structure: Basic Theory and Practical Methods* (Cambridge University Press)
- [36] Saito R, Dresselhaus G and Dresselhaus M S 2003 *Physical Properties of Carbon Nanotubes* (London, Imperial College Press)
- [37] Yu M F, Files B S, Arepalli S and Ruoff R S 2000 *Phys. Rev. Lett.* **84** 5552
- [38] Lu J P 1997 *Phys. Rev. Lett.* **79** 1297
- [39] Li Y, Qiu X, Yin Y, Yang F and Fan Q 2009 *Phys. Lett. A* **373** 2368
- [40] Grantab R, Shenoy V B and Ruoff R S 2010 *Science* **330** 946
- [41] Zhao H, Min K and Aluru N R 2009 *Nano Lett.* **9** 3012
- [42] Yu M F, Lourie O, Dyer M J, Moloni K, Kelly T F and Ruoff R S 2000 *Science* **287** 637
- [43] Lee S M, An K H, Lee, Y H, Seifert G and Frauenheim T 2001 *J. Am. Chem. Soc.* **123** 5059